applied optics

Broadband mid-infrared fiber optical parametric oscillator based on a three-hole suspended-core chalcogenide fiber

HANGYU BAI, XIONG YANG, YIZHEN WEI, AND SHIMING GAO*

Centre for Optical and Electromagnetic Research, State Key Laboratory of Modern Optical Instrumentation, Zhejiang University, Hangzhou 310058, China
**Corresponding author: gaosm@zju.edu.cn*

Received 8 October 2015; revised 10 December 2015; accepted 10 December 2015; posted 15 December 2015 (Doc. ID 251600); published 14 January 2016

A mid-infrared fiber optical parametric oscillator is proposed and designed based on a three-hole As_2S_5 suspended-core fiber (SCF). The eigenmodes of the SCF are depicted and the pump condition for single-mode operation is analyzed. The zero-dispersion wavelength is shifted to 2 μm by tuning the core diameter of the SCF. Using the degenerate four-wave mixing coupled-wave equations, a tuning range of the idler wavelength from 2 to 5 μm and a maximum conversion efficiency of 19% are numerically predicted in a 0.1-m-long SCF pumped by a 2.7 W thulium-doped fiber laser.

OCIS codes: (140.3070) Infrared and far-infrared lasers; (190.4380) Nonlinear optics, four-wave mixing; (060.3510) Lasers, fiber; (060.4005) Microstructured fibers.

http://dx.doi.org/10.1364/AO.55.000515

1. INTRODUCTION

The mid-infrared (MIR) band mainly from 2 to 5 μm has attracted lots of interest due to its various applications in spectroscopy, medicine, and military. In the MIR band, lasing can be generated through several typical ways, such as a rare-earth-doped fiber laser, quantum cascade laser, cascaded Raman laser, and optical parametric oscillator (OPO) [1–4]. Compared with other methods, an OPO, using a pump to generate a pair of signal and idler through four-wave mixing (FWM) in a cavity, shows more advantages in broadband tunability. A tunable band from 2.6–6.1 μm has been demonstrated in a GaAs crystal-based OPO pumped by thulium-doped fiber laser (TDFL) [5]. Using a periodically poled lithium niobate crystal, an OPO slope efficiency as high as 19.1% at 3.84 μm has been achieved [6].

Compared with nonlinear crystals, highly nonlinear fibers exhibit more stability and flexibility for OPO applications since the fiber dispersion determines that the OPO gain spectrum can be engineered. Therefore, fiber OPOs (FOPOs) that use optical fibers as the nonlinear media have attracted a lot of interest. In a dispersion-shifted fiber, an oscillation wavelength as long as 2140 nm has been realized and the wavelength limit is mainly due to the large intrinsic loss of fused silica above 2 μm [7]. In the MIR region, chalcogenide glass fibers are promising due to their low intrinsic loss and high nonlinearity [8]. Also, chalcogenide fibers have features including much less flexure and shear strength compared to silica fiber [9]. However, the zero material dispersion wavelengths of bulk chalcogenide glasses locate around 5 μm or even longer. In order to obtain the oscillation wavelength in the 2–5 μm region the pump wavelength should be 2 μm or even shorter according to energy conservation of the FWM process. Correspondingly, the zero-dispersion wavelength (ZDW) needs to be near the pump for phase matching [10,11]. An effective way to shift the ZDW is to design chalcogenide fiber structures by introducing high waveguide dispersion to compensate the material dispersion. Using the high nonlinearity and low loss of chalcogenide fibers, soliton self-frequency shift and supercontinuum generation have been demonstrated in the MIR region [12,13]. Recently, parametric amplification and oscillation have been demonstrated in As_2Se_3 chalcogenide microwires in the telecommunication window by tuning its ZDW to around 1536 nm, where a total slope efficiency of 19% was obtained [14,15]. Moreover, far-detuned MIR frequency conversion via normal dispersion modulation instability has been observed, which showed the possibility to realize MIR FOPO using chalcogenide microwires [16]. Compared to microwires, microstructured fibers have stronger ability to tune their dispersion profiles. A FOPO based on a tellurite photonic crystal fiber has been numerically studied, and a MIR-tunable range from 1.6 to 4 μm and a conversion efficiency of 10% was predicted [17]. Moreover, it has been demonstrated that the suspended-core structure is a feasible way to realize

wideband ZDW shift [18]; therefore, suspended-core fibers (SCFs) become an important choice for MIR FOPO. Using a suspended-core tellurite microstructured optical fiber pumped by a mode-locked erbium-doped fiber laser, a FOPO has been experimentally demonstrated, whose oscillated signal can be generated from 1606 to 1743.5 nm, and an idler can be emitted from 1526.8 to 1395 nm by adjusting the pump wavelength from 1565.4 to 1551 nm [19].

In order to move the ZDW of the SCF to a shorter wavelength, the fiber core diameter has to be reduced. However, the reduction of diameter will bring more difficulty in fiber fabrication. A reasonable way is to use a pump whose wavelength is as long as possible. As mentioned above, in order to tune the idler wavelength in the 2–5 μm region, the pump wavelength should be 2 μm or even shorter. Therefore, it seems to be the best solution to choose a pump with a wavelength of around 2 μm. Fortunately, TDFLs have exactly provided high-quality pump sources in the 2 μm band. For instance, a thulium-doped fiber amplifier system has been demonstrated to produce 100 kW peak power picosecond pulse at 2 μm [20], and a TDFL providing >150 W of average power, >50% slope efficiency, and >100 nm tunability around 2 μm has also been realized [21]. Via TDFLs, high-quality lasing from 1.8 to 2.1 μm with high average power and high slope efficiency can be provided.

Chalcogenide glass fibers can be classified into several typical categories according to their materials, wherein tellurite fibers suffer from strong water absorption in the infrared range [9], and selenide fibers need a core diameter as small as 1 μm to shift the ZDW to 2 μm. After comparison, sulfide fibers specified as As_2S_5 fibers are chosen for MIR FOPO due to their wide transmission window and relative large core diameter when the ZDW is 2 μm. In this paper, we proposed a MIR FOPO based on a three-hole As_2S_5 SCF. When the core diameter of the SCF is tuned to 2.6 μm, the ZDW is tuned to 2 μm. By tuning the TDFL from 1.9 to 2 μm, an ultrawide tuning range of the idler wavelength can be numerically obtained, which covers the entire 2–5 μm band. After analyzing the eigenmodes in the SCF, it is found to be possible that only one single transverse mode is excited in the fiber by carefully adjusting the input polarization angle of the pump. In such a MIR FOPO system, a maximum conversion efficiency of 19% for the idler wavelength is predicted.

2. DESIGN OF THE THREE-HOLE SCF

In order to shift the ZDW of the chalcogenide fiber to around 2 μm, we choose the three-hole suspended structure as the basic structure to design the gain medium of the FOPO, as shown in Fig. 1(a). The chalcogenide material is selected to be As_2S_5. In Fig. 1(a), the fiber structure consists of a chalcogenide fiber core with three bridges, which forms three air holes together with the outside wall. The suspended core is enlarged in Fig. 1(b) since almost all of the electrical field is confined in this area. The suspended-core diameter is denoted as d, which is used to tune the ZDW of the SCF, and the width of the bridge is denoted as w, which is fixed as 0.6 μm. A perfect matching layer is added for simulation convenience, which is used to absorb the redundant optical field when using the COMSOL

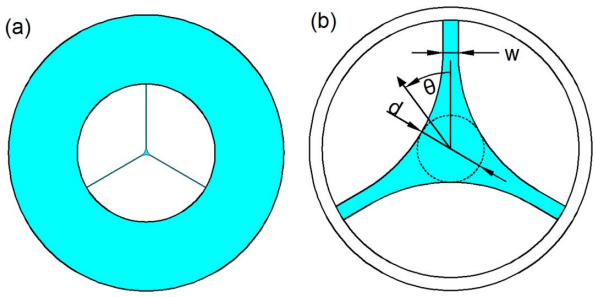

Fig. 1. Geometrical structure of the As_2S_5 three-hole SCF: (a) cross section of the whole fiber, (b) the enlarged core area for simulation.

software for simulation, and has a diameter of 10.5 μm and a thickness of 1 μm.

The proposed three-hole SCF shows the multimode feature when the waveguide dispersion is anomalous [18]. By using the finite element method of COMSOL, the mode field distributions of all the modes in the fiber can be obtained. Figure 2 shows six mode distributions of the eigenmodes in the SCF at 1.95 μm when the fiber diameter d is fixed at 2.6 μm. The six modes are denoted as Mode1–Mode6, which are ranked by their effective refractive indices from large to small. The arrows in the mode distributions show the vectors of the electric fields distributed in the cross sections. In the six modes, one can find that modes Mode1 and Mode2 have similar mode distributions, and they share the same effective refractive index, indicating that they form a degenerate pair of modes. Mode4 and Mode5 are also a degenerate pair of modes as they follow the same rules compared with Mode1 and Mode2. Mode1 and Mode2 are two fundamental modes with their polarization states perpendicular to each other. Since their electric vectors point to certain directions, the boundary conditions on the three interfaces are different, which makes their field distributions both asymmetrical.

The effective refractive indices can be obtained for all the modes in the SCF using the material dispersion data of As_2S_5 [12]. And then the dispersion curves are calculated from the differentials of the effective refractive indices. In Fig. 3, the corresponding dispersion curves for each mode of the 2.6-μm-diameter SCF are depicted; the dispersions of Mode1 and Mode2 overlap with each other, and the dispersions of Mode4 and Mode5 overlap with each other.

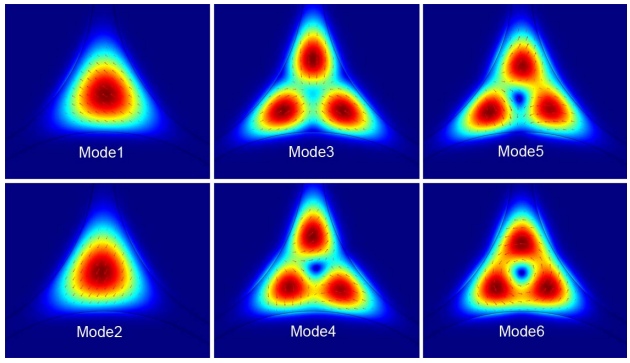

Fig. 2. Mode field distributions of the six eigenmodes in the three-hole SCF at 1.95 μm.

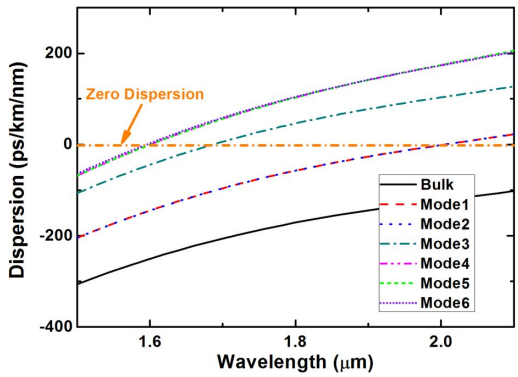

Fig. 3. Dispersion curves for the six modes Mode1–Mode6 as the wavelength varies.

For a chalcogenide fiber, the typical coupling method is free-space coupling or butt coupling since it is fragile and hard to be spliced to other kinds of fibers. In this case, the coupling efficiencies will be different for various modes according to the pump condition. It is essential to quantitatively analyze each mode coupling efficiency as the pump varies. Assuming the linearly polarized pump beam with a Gaussian profile on the cross section, whose diameter is 4 μm, is focused on the core center precisely. In order to describe the polarization state of a light in the SCF, the polarization angle θ is defined as the anticlockwise rotated angle from the vertical bridge of the SCF, as shown in Fig. 1(b). And then we calculated the coupling efficiency for Mode1–Mode6 [22]. The results are listed in Table 1. The total coupling efficiency is not large due to the leakage of energy in the case of a relative large diameter of pump compared to the core diameter, and none of the high-order modes is excited. There is other useful information that most of the energy has been coupled to Mode1 when the polarization angle is 60°. This indicates that one single transverse mode can be excited by carefully adjusting the input polarization angle. Table 2 shows the coupling efficiency when there is a displacement of the injected pump location of 0.5 μm. One can see that the influence of the displacement is very slight except for a small amount of efficiency reduction. As a result, one single transverse mode can be achieved by carefully adjusting the input polarization angle and the focusing point.

Figure 4 shows the obtained ZDW of the Mode1 in the SCF as the core diameter d varies. One can find that the ZDW will move to a shorter wavelength as the core diameter reduces, and a ZDW near 2 μm can be obtained when the core diameter is reduced to 2.6 μm, which can be used as the nonlinear medium for a MIR FOPO pumped by a TDFL.

3. THEORETICAL MODEL

The MIR FOPO configuration for a simulation based on a three-hole SCF is illustrated in Fig. 5, where a TDFL is used as the pump source, the polarization controller after the pump is used to optimize its polarization state to maximum the conversion efficiency, and a single resonant cavity is designed that ensures the signal light resonant in the cavity and keeps other lights single passing the gain medium. The resonant cavity consists of four mirrors: M1, M2, M3, and M4. All of these mirrors are of high reflectivity at the signal wavelength. M1 is antireflective at the pump wavelength, and M2 is antireflective at the idler wavelength.

For a SCF with a core diameter of 2.6 μm, the ZDW is 2 μm for the fundamental modes: Mode1 and Mode2. In a FOPO, the output signal and idler wavelengths are determined by the effective phase-matching condition once the pump wavelength is fixed. The effective phase-matching condition can be expressed as

$$\kappa = \Delta\beta + 2\gamma_p P_p = \beta_s + \beta_i - 2\beta_p + 2\gamma_p P_p = 0, \quad (1)$$

where κ is the effective phase mismatch of the four interactive waves; $\Delta\beta$ is the phase mismatch of the four interactive waves; $\beta_{p,s,i}$ are the propagation constants of the pump, signal, and idler lights, respectively; γ_p is the nonlinear parameter for pump wavelength; and P_p is the pump power. For a certain pump wavelength, a pair of signal and idler wavelengths can be calculated by solving Eq. (1), which means that the

Table 1. Calculated Mode Coupling Efficiency of the Six Modes under Different Polarization Angles

		Mode Coupling Efficiency [%]					
Polarization Angle [deg]	Total Coupling Efficiency [%]	Mode1	Mode2	Mode3	Mode4	Mode5	Mode6
0	45.8	13.1	32.7	0	0	0	0
30	45.8	35.9	9.9	0	0	0	0
60	45.8	45.7	0.1	0	0	0	0
90	45.8	32.7	13.1	0	0	0	0

Table 2. Calculated Mode Coupling Efficiency of the Six Modes under Different Polarization Angles for the Case of the Focusing Light with a Displacement of 0.5 μm

		Mode Coupling Efficiency [%]					
Polarization Angle [deg]	Total Coupling Efficiency [%]	Mode1	Mode2	Mode3	Mode4	Mode5	Mode6
0	45	12.7	31.7	0.3	0.3	0	0
30	44.6	34.2	9.8	0.2	0.2	0.1	0.1
60	43.7	43.2	0	0.1	0	0.2	0.2
90	43.3	30.6	12.2	0	0	0.2	0.3

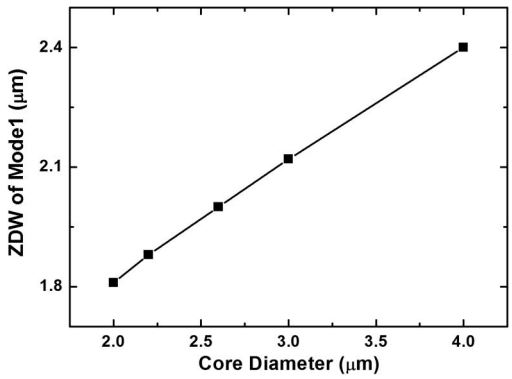

Fig. 4. ZDW of the SCF as a function of the core diameter.

phase-matching condition is completely satisfied. In this case, the signal and idler can get the maximum parametric gain. However, for the signal and idler near this pair of completely phase-matched wavelengths, the parametric gain will drop gradually, as shown in Fig. 6, where the normalized parametric gain of Mode1 is simulated as a function of the pump wavelength. The signal and idler wavelengths that can be obtained are also illustrated according to the effective phase-matching condition. One can find that the idler wavelength can vary from 2 to 5 μm if a TDFL with a tuning range of 1.9–2 μm is used as the pump. When the pump wavelength is located in the normal dispersion region, it has to be a little far from the ZDW to satisfy the effective phase-matching condition. Since $\Delta\beta$ changes rapidly with pump wavelength in this case and the range over which the parametric gain exists is given by $0 > \Delta\beta > -4\gamma P$, the pump wavelength satisfying this equation has been limited to a narrow region. This character can be observed from Fig. 6 that both the created signal and idler lights have narrow bandwidths when the pump wavelength locates in the normal dispersion region of the SCF [11].

The influence of the high-order modes are also verified in the point of view of the effective phase-matching condition. Figure 7 shows the effective phase-matching conditions for all six modes Mode1–Mode6. One can find that the required pump wavelengths for the high-order modes Mode3–Mode6 to meet the effective phase-matching conditions are quite different from that of Mode1 and Mode2. It shows that no phase-matched signal or idler wavelength exists for Mode3–Mode6 when the pump wavelength is tuned from 1.8 to 2.1 μm.

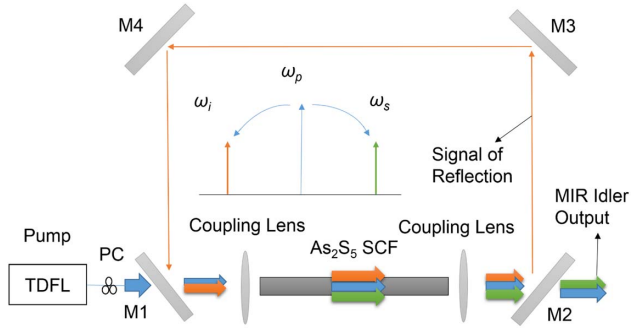

Fig. 5. Configuration of the proposed MIR FOPO based on the SCF.

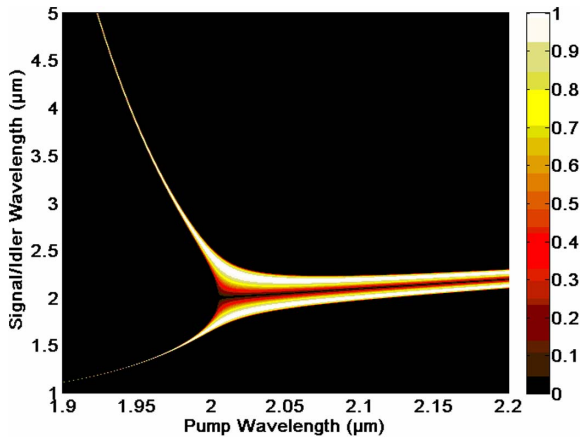

Fig. 6. Normalized parametric gain of the SCF as a function of the pump, generated signal, and idler wavelengths with a pump power of $P = 10$ W.

As a result, the signal and idler can be effectively generated without the influence of the high-order modes. On the other hand, the strongly suppression of the intermodal FWM has been demonstrated due to the large phase mismatch and will not transfer energy to an initially empty high-order mode under the suspended-core structure [23], while the two degenerate modes Mode1 and Mode2 can still transfer energy to each other. It is reasonable to only consider the FWM processes of the fundamental modes Mode1 and Mode2 to evaluate the performance of the MIR FOPO.

According to Table 1, the incident pump power will be maintained in Mode1 if the polarization state of the pump is tuned to 60°. Since the FWM effect is polarization sensitive, the generated signal and idler will be copolarized with the pump, that is, they are also in the M1 mode. In this case, the coupled-wave equations for the MIR FOPO can be expressed as [24]

$$\frac{\partial A_p}{\partial z} + \frac{i}{2}\beta_{2p}\frac{\partial^2 A_p}{\partial t^2} + \frac{1}{2}\alpha_p A_p = i\gamma_p[(|A_p|^2 + 2|A_s|^2 + 2|A_i|^2)A_p + 2A_s A_i A_p^* e^{i\Delta\beta z}], \quad (2)$$

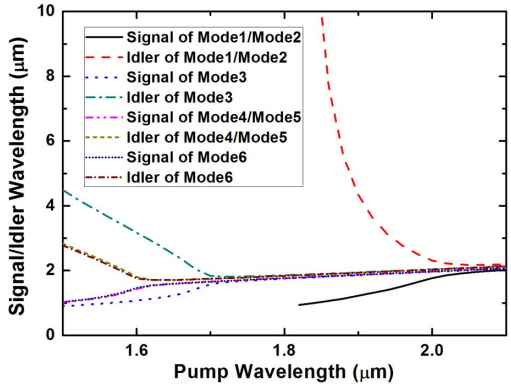

Fig. 7. Phase-matched signal and idler wavelengths as functions of the pump wavelength for Mode1–Mode6 at the pump power of $P = 10$ W.

$$\frac{\partial A_s}{\partial z}+\frac{i}{2}\beta_{2s}\frac{\partial^2 A_s}{\partial t^2}+\frac{1}{2}\alpha_s A_s = i\gamma_s[(|A_s|^2+2|A_p|^2+2|A_i|^2)A_s+2A_p^2A_i^*e^{-i\Delta\beta z}], \quad (3)$$

$$\frac{\partial A_i}{\partial z}+\frac{i}{2}\beta_{2i}\frac{\partial^2 A_i}{\partial t^2}+\frac{1}{2}\alpha_i A_i = i\gamma_i[(|A_i|^2+2|A_p|^2+2|A_s|^2)A_i+2A_p^2A_s^*e^{-i\Delta\beta z}], \quad (4)$$

where $A_{p,s,i}$, $\omega_{p,s,i}$, $\beta_{2p,s,i}$, $\gamma_{p,s,i}$, and $\alpha_{p,s,i}$ are the amplitude, the angular frequency, the second-order group-velocity dispersion, the nonlinear parameter, and the loss coefficient of the SCF for the pump, signal, and idler lights, respectively. $\Delta\beta=\beta_s+\beta_i-2\beta_p$ is the phase mismatch, where $\beta_{p,s,i}$ are the propagation constants of the pump, signal, and idler lights, respectively. Taking two-photon absorption (TPA) into consideration, the nonlinear parameter [25] is expressed as

$$\gamma_j=\frac{n_2\omega_j}{cA_{\text{eff}}}+i\frac{\beta_{\text{TPA}}}{2A_{\text{eff}}}, \qquad (j=p,s,i), \quad (5)$$

where n_2 is the nonlinear refractive index coefficient, c is the velocity of light in vacuum, β_{TPA} is the TPA coefficient, and A_{eff} is the effective mode area,

$$A_{\text{eff}}=\frac{\left[\int\int_{-\infty}^{\infty}|F(x,y)|^2\mathrm{d}x\mathrm{d}y\right]^2}{\int\int_{-\infty}^{\infty}|F(x,y)|^4\mathrm{d}x\mathrm{d}y}, \quad (6)$$

where $F(x,y)$ is the normalized mode distribution.

Assuming that the pump is provided by a nanosecond pulse laser, it can be considered as a quasi-CW pump and the time derivative in the coupled-wave equation can be ignored. The cavity length can be tuned by moving the two mirrors M3 and M4 to ensure the synchronization between the pump and the signal light. Therefore, the phase of the signal light at the beginning of every round trip is set as 0. For such a FOPO configuration, the coupled-wave equations satisfy the following boundary conditions,

$$A_s(z=0,t)=\sqrt{1-\alpha_{\text{linear}}}|A_s(z=L,t)|$$
$$A_p(z=0,t)=\sqrt{P_p}, \quad (7)$$

where P_p is the input pump power, α_{linear} is the additional cavity loss excluding the fiber loss at the signal wavelength (i.e., introduced by the mirrors and the fiber coupling), and L is the length of the SCF. With these boundary conditions, the coupled-wave equations can be solved using iterative algorithms. The generated signal and idler powers can be numerically obtained.

4. RESULTS AND DISCUSSION

The above coupled-wave equations are solved using a home-built fourth-order Adams–Bashforth method. The pump wavelength is assumed to be 1.95 μm, and the phase-matched signal and idler wavelengths are calculated to be 1.318 and 3.749 μm, respectively. In this case, the performance of the MIR FOPO is analyzed. In the simulation, $n_2=0.54\times10^{-17}$, $A_{\text{eff}s}=4.308\ \mu\text{m}^2$, $A_{\text{eff}p}=4.646\ \mu\text{m}^2$, $A_{\text{eff}i}=6.113\ \mu\text{m}^2$, $\beta_{\text{TPA}s}=0.102$ cm/GW, $\beta_{\text{TPA}p}=0.0072$ cm/GW, $\beta_{\text{TPA}i}=5\times10^{-5}$ cm/GW [26], $\alpha_s=\alpha_p=\alpha_i=1$ dB/m [8], $\alpha_{\text{linear}}=50\%$, and $\Delta\beta=-2\gamma_pP_p$.

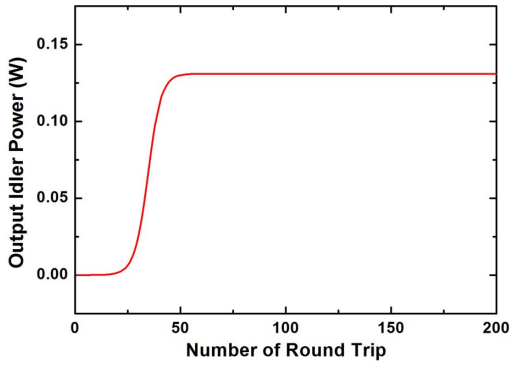

Fig. 8. Output power of MIR idler as a function of the number of signal round trip for $P_p=1$ W and $L=0.2$ m.

To verify the stability of the model, the number of cycles for oscillation is simulated, as shown in Fig. 8. The signal eventually reaches stable oscillation when the incident pump power $P_p=1$ W and the SCF length is $L=0.2$ m. The stable MIR output power of the idler is 0.131 W. Figure 9 shows the pump threshold of the FOPO as a function of the fiber length. Increasing the SCF length from 0.01 to 1 m, the threshold pump peak power sharply decreases from 16 to 0.21 W. It means that the requirement to the pump power will be reduced if a longer SCF is used.

The output idler power is calculated as a function of pump power, as shown in Fig. 10, where the fiber length is 0.1 or 0.06 m, respectively. The saturation effect of the pump power is observed and an optimal pump power exists to obtain the highest output idler power for different fiber lengths. Here the conversion efficiency is defined as the ratio of the output idler power with respect to the input pump power. It is shown that the pump power and the SCF length should be optimized simultaneously to achieve the maximum conversion efficiency. And then we sweep the pump power when the fiber length is fixed and calculate its maximum conversion efficiency. After computing under different fiber lengths, the obtained maximum conversion efficiency is depicted as a function of the sampled fiber length, as shown in Fig. 11. At the same time, the corresponding incident pump power to acquire the maxi-

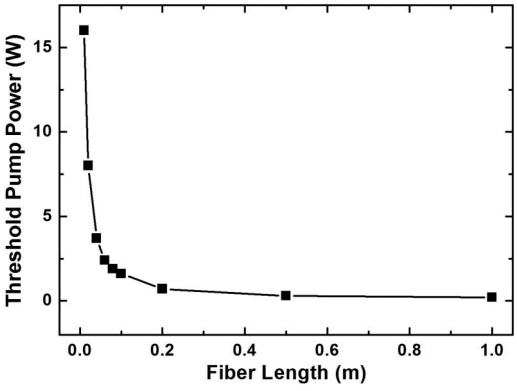

Fig. 9. Threshold of the pump power as a function of the fiber length.

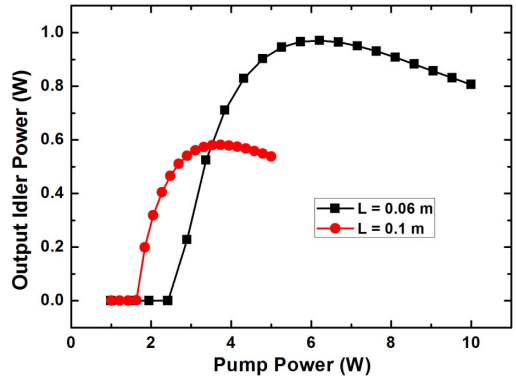

Fig. 10. Output idler power as a function of the pump power.

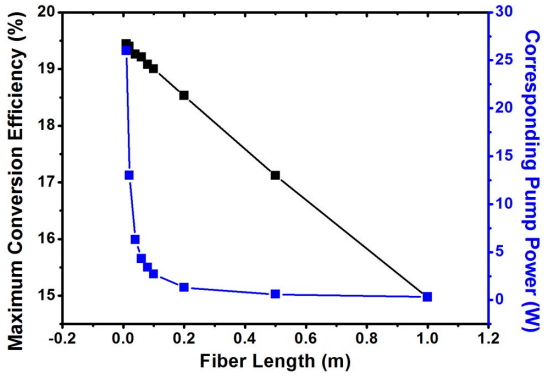

Fig. 11. Maximum conversion efficiency and the corresponding pump power as a function of the fiber length.

mum conversion efficiency is also shown. One can see that the maximum conversion efficiency of the idler light drops with the increasing of the fiber length, which is mainly due to the increasing of the fiber loss. For a 0.1 m long SCF, the conversion efficiency of 19% in the MIR band can be achieved when the incident pump power is 2.7 W. Comparing with other relative works, the predicted conversion efficiency is still expected. For example, a conversion efficiency of 10% was simulated in a tellurite FOPO in the MIR band [17], and a conversion efficiency of 13% was measured in a chalcogenide OPO demonstrated in the telecommunication band [15]. The efficiency can be further improved if the cavity loss can be effectively reduced.

5. CONCLUSIONS

A MIR FOPO based on a three-hole As_2S_5 SCF has been proposed. The dispersion of the SCF is engineered to have a ZDW at 2 μm by tuning the core diameter to be 2.6 μm in order to use a TDFL as the pump. The eigenmodes of the SCF and their dispersion performances are analyzed. By carefully choosing the polarization angle of the incident pump, one can only excite a single transverse mode. The idler wavelength can cover 2–5 μm by tuning the TDFL from 1.9 to 2 μm. A maximum conversion efficiency of 19% for the idler wavelength is numerically predicted in a 0.1-m-long SCF with an incident pump power of 2.7 W.

Funding. Natural Science Foundation of Zhejiang Province (LY14F050006); Fundamental Research Funds for the Central Universities (2015FZA5003); National Natural Science Foundation of China (NSFC) (61475138, 61178001); China Postdoctoral Science Foundation (2014M551730); Specialized Research Fund for the Doctoral Program of Higher Education of China (20130101110089).

REFERENCES

1. Y. Wei, K. Hu, B. Sun, and T. Wang, "All-fiber widely wavelength-tunable thulium-doped fiber ring laser incorporating a Fabry-Perot filter," Laser Phys. **22**, 770–773 (2012).
2. B. Meng and Q. J. Wang, "Broadly tunable single-mode mid-infrared quantum cascade lasers," J. Opt. **17**, 023001 (2015).
3. H. Rong, S. Xu, O. Cohen, O. Raday, M. Lee, V. Sih, and M. Paniccia, "A cascaded silicon Raman laser," Nat. Photonics **2**, 170–174 (2008).
4. K. C. Burr, C. L. Tang, M. A. Arbore, and M. M. Fejer, "Broadly tunable mid-infrared femtosecond optical parametric oscillator using all-solid-state-pumped periodically poled lithium niobate," Opt. Lett. **22**, 1458–1460 (1997).
5. N. Leindecker, A. Marandi, R. L. Byer, K. L. Vodopyanov, J. Jiang, I. Hartl, M. Fermann, and P. G. Schunemann, "Octave-spanning ultrafast OPO with 2.6–6.1 μm instantaneous bandwidth pumped by femtosecond Tm-fiber laser," Opt. Express **20**, 7046–7053 (2012).
6. Y. Peng, W. Wang, X. Wei, and D. Li, "High-efficiency mid-infrared optical parametric oscillator based on PPMgO:CLN," Opt. Lett. **34**, 2897–2899 (2009).
7. A. Gershikov, E. Shumakher, A. Willinger, and G. Eisenstein, "Fiber parametric oscillator for the 2 μm wavelength range based on narrow-band optical parametric amplification," Opt. Lett. **35**, 3198–3200 (2010).
8. I. Savelii, O. Mouawad, J. Fatome, B. Kibler, F. Désévédavy, G. Gadret, J.-C. Jules, P.-Y. Bony, H. Kawashima, W. Gao, T. Kohoutek, T. Suzuki, Y. Ohishi, and F. Smektala, "Mid-infrared 2000-nm bandwidth supercontinuum generation in suspended-core microstructured sulfide and tellurite optical fibers," Opt. Express **20**, 27083–27093 (2012).
9. J. A. Harrington, "Chalcogenide glass fiber optics," in *Infrared Fibers and Their Applications* (SPIE, 2004), pp. 83–104.
10. M. E. Marhic, N. Kagi, T.-K. Chiang, and L. G. Kazovsky, "Broadband fiber optical parametric amplifiers," Opt. Lett. **21**, 573–575 (1996).
11. M. E. Marhic, K. K. Wong, and L. G. Kazovsky, "Wide-band tuning of the gain spectra of one-pump fiber optical parametric amplifiers," J. Sel. Top. Quantum Electron. **10**, 1133–1141 (2004).
12. T. Cheng, R. Usaki, Z. Duan, W. Gao, D. Deng, M. Liao, Y. Kanou, M. Matsumoto, T. Misumi, T. Suzuki, and Y. Ohishi, "Soliton self-frequency shift and third-harmonic generation in a four-hole As_2S_5 microstructured optical fiber," Opt. Express **22**, 3740–3746 (2014).
13. A. Al-kadry, C. Baker, M. E. Amraoui, Y. Messaddeq, and M. Rochette, "Broadband supercontinuum generation in As_2Se_3 chalcogenide wires by avoiding the two-photon absorption effects," Opt. Lett. **38**, 1185–1187 (2013).
14. R. Ahmad and M. Rochette, "High efficiency and ultra broadband optical parametric four-wave mixing in chalcogenide-PMMA hybrid microwires," Opt. Express **20**, 9572–9580 (2012).
15. R. Ahmad and M. Rochette, "Chalcogenide optical parametric oscillator," Opt. Express **20**, 10095–10099 (2012).
16. T. Godin, Y. Combes, R. Ahmad, M. Rochette, T. Sylvestre, and J. M. Dudley, "Far-detuned mid-infrared frequency conversion via normal dispersion modulation instability in chalcogenide microwires," Opt. Lett. **39**, 1885–1888 (2014).
17. H. Cheng, Z. Luo, C. Ye, Y. Huang, C. Liu, and Z. Cai, "Numerical modeling of mid-infrared fiber optical parametric oscillator based on the degenerated FWM of tellurite photonic crystal fiber," Appl. Opt. **52**, 525–529 (2013).
18. L. Dong, B. K. Thomas, and L. Fu, "Highly nonlinear silica suspended core fibers," Opt. Express **16**, 16423–16430 (2008).

19. L. Zhang, T. H. Tuan, H. Kawamura, T. Suzuki, and Y. Ohishi, "Optical parametric oscillator based on degenerate four-wave mixing in suspended core tellurite microstructured optical fiber," Opt. Express **23**, 26299–26304 (2015).
20. A. M. Heidt, Z. Li, J. Sahu, P. C. Shardlow, M. Becker, M. Rothhardt, M. Ibsen, R. Phelan, B. Kelly, S. U. Alam, and D. J. Richardson, "100 kW peak power picosecond thulium-doped fiber amplifier system seeded by a gain-switched diode laser at 2 μm," Opt. Lett. **38**, 1615–1617 (2013).
21. T. S. McComb, R. A. Sims, C. C. C. Willis, P. Kadwani, V. Sudesh, L. Shah, and M. Richardson, "High-power widely tunable thulium fiber lasers," Appl. Opt. **49**, 6236–6242 (2010).
22. M. Grabka, B. Wajnchold, S. Pustelny, W. Gawlik, K. Skorupski, and P. Mergo, "Experimental and theoretical study of light propagation in suspended-core optical fiber," Acta Phys. Pol. A **118**, 1127–1132 (2010).
23. I. Shavrin, S. Novotny, and H. Ludvigsen, "Mode excitation and supercontinuum generation in a few-mode suspended-core fiber," Opt. Express **21**, 32141–32150 (2013).
24. G. P. Agrawal, *Nonlinear Fiber Optics* (Academic, 2007).
25. Q. Lin, O. J. Painter, and G. P. Agrawal, "Nonlinear optical phenomena in silicon waveguides: modeling and applications," Opt. Express **15**, 16604–16644 (2007).
26. M. J. Weber, "Glasses," in *Handbook of Optical Materials* (CRC Press, 2003), p. 281.